

# Optical frequency measurements of $6s\ ^2S_{1/2}-6p\ ^2P_{1/2}$ ( $D_1$ ) transitions in $^{133}\text{Cs}$ and their impact on the fine-structure constant

V. Gerginov, K. Calkins, and C. E. Tanner\*

*Department of Physics, University of Notre Dame, Notre Dame, Indiana 46556-5670, USA*

J. J. McFerran

*School of Physics, The University of Western Australia, 35 Stirling Highway, Nedlands, 6009, Australia*

S. Diddams, A. Bartels, and L. Hollberg

*Time and Frequency Division, National Institute of Standards and Technology, 325 Broadway M.C. 847, Boulder Colorado 80305, USA*

(Received 24 August 2005; published 8 March 2006)

High resolution laser spectroscopy of the  $6s\ ^2S_{1/2}\rightarrow 6p\ ^2P_{1/2}$  transition ( $D_1$  line) in neutral  $^{133}\text{Cs}$  is performed in a highly collimated thermal atomic beam by use of a femtosecond laser frequency comb and narrow-linewidth diode laser. The diode laser is offset locked to a single frequency component of the femtosecond laser frequency comb and probes the optical transitions between selected pairs of ground-state and excited-state hyperfine components. A photodiode detects the excited-state decay fluorescence, and a computerized data acquisition system records the signal. The Doppler shift is eliminated by orienting the laser beam in a direction perpendicular to the atomic beam to within a precision of  $5\times 10^{-6}$  rad. Optical frequencies for all four pairs of hyperfine components are measured independently, from which the  $D_1$  line centroid and excited-state hyperfine splitting are obtained by least-squares minimization with the ground-state splitting as a fixed constraint. We find the  $D_1$  line centroid to be  $f_{D_1}=335\,116\,048\,748.1(2.4)$  kHz, and the  $6p\ ^2P_{1/2}$  state hyperfine splitting to be  $1\,167\,723.6(4.8)$  kHz. These results, in combination with the results of an atom interferometry experiment by Wicht *et al.* [Phys. Scripta T **102**, 82 (2002)], are used to calculate a new value for the fine-structure constant.

DOI: [10.1103/PhysRevA.73.032504](https://doi.org/10.1103/PhysRevA.73.032504)

PACS number(s): 32.10.Fn, 42.62.Fi, 06.30.Ft, 06.20.Jr

## I. INTRODUCTION

Precision measurement techniques developed in recent years have provided us with ways to test fundamental theories in areas that lie outside atomic physics. Tests of the standard model, a value of the fine-structure constant  $\alpha$ , measurements of nuclear structure, and the weak interaction are all possible using accumulated information about transition amplitudes and frequencies obtained through precise measurements [2–5]. Cesium, being one of the most thoroughly studied heavy atoms, is very suitable for these investigations, since the accuracy of atomic theory in this system is on the order of 1% [6]. In this respect, measurements of transition frequencies play a very important role because the experimental accuracy can be many orders of magnitude better than accuracies obtained through atomic structure calculations. The results and level of accuracy obtained for the absolute transition frequencies presented here are of particular relevance to the interpretation of atom interferometry experiments involving cesium, where the recoil energy and momentum transfer of single-photon interactions are required. Examples of physics expected from combining absolute transition frequencies with atom interferometry include measurements of local gravity [7] and a value for the fine-structure constant [1].

A variety of techniques have been implemented to eliminate Doppler effects in optical frequency measurements of

atomic transitions. These include saturated absorption spectroscopy in vapor cells [3,8], magneto-optic traps [9], and thermal atomic beams [10,11]. While vapor cell experiments are easier to implement, the laser intensity must be high enough to produce a saturated absorption spectrum. The high laser intensity causes systematic effects due to optical pumping, magnetic fields, and light pressure, which limit the final uncertainty. In previous measurements of the  $6s\ ^2S_{1/2}\rightarrow 6p\ ^2P_{1/2}$  transition in  $^{133}\text{Cs}$ , the final uncertainty was limited by such systematic effects and not by optical frequency measurement techniques [3]. In atomic beams, Doppler broadening can be reduced geometrically to less than the natural linewidth for allowed transitions, where its effect on determining the spectral line centers is significantly reduced. In addition, optical pumping can be suppressed by working at low light intensity. With atomic beams, the most serious experimental problem is often the shift of the optical resonances caused by the Doppler effect when the projection of the atomic velocities along the laser beam direction of propagation is not zero. This shift can be significantly reduced in magneto-optic traps because of the reduced atomic velocities, at the expense of a much more complicated system, reduced signal size and issues with optical forces inducing atomic motion [12]. In this work, we show that with a simple experimental procedure and careful control of experimental parameters, the Doppler shift caused by atomic and laser beam misalignment can be reduced to the level of other uncertainties.

\*Electronic address: Carol.E.Tanner.1@nd.edu

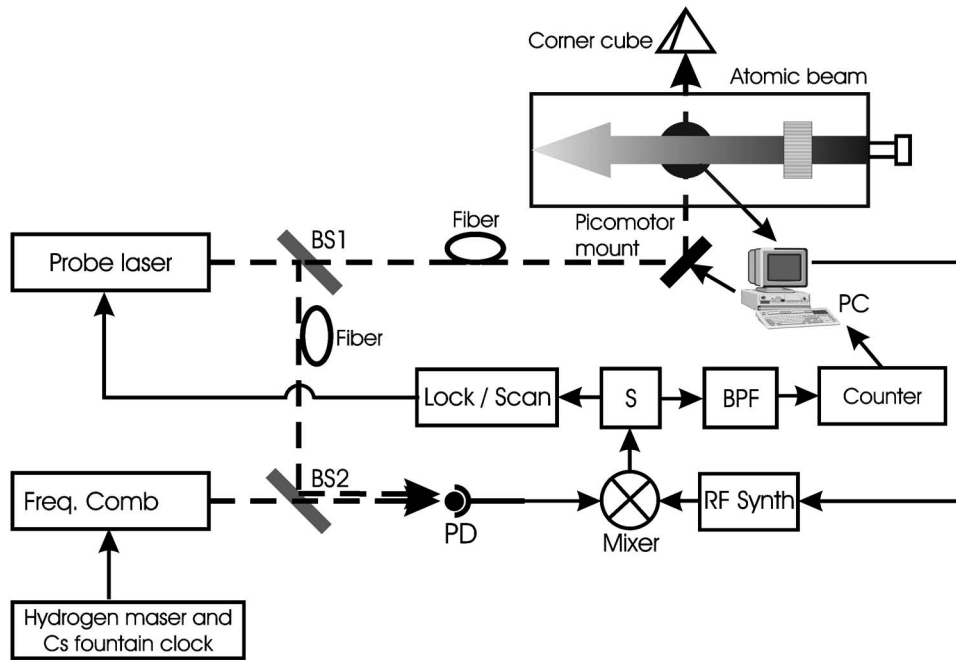


FIG. 1. Experimental setup.

## II. EXPERIMENTAL SETUP

The experimental setup is shown in Fig. 1. A probe diode laser system emitting 895 nm light is used to excite a highly collimated atomic beam perpendicular to the beam direction. The fluorescence of the excited atoms is recorded with a data acquisition system (DAQ). Part of the probe laser output is mixed with the output of a Ti:sapphire femtosecond laser frequency comb (FLFC). The probe laser frequency is offset locked to a specific comb component and is scanned by changing the offset frequency. A frequency counter measures the probe laser frequency detuning. Atomic and laser beam misalignment is measured and eliminated using information from spectra with one and two counter-propagating laser beams.

### A. Diode laser system

The single mode 8 mW diode laser has a free running linewidth of 15 MHz. Its linewidth is narrowed using optical feedback from a 10 cm long Fabry-Pérot cavity (finesse of 100, defined as free spectral range divided by fringe width) using the method of Dahmani *et al.* [13]. A beam splitter reflects 50% of the laser output into the cavity. A lens places the beam waist in the center of the cavity. The laser current is modulated at 27 kHz and phase detection is used to control the optical path length between the laser and the confocal cavity by detecting the light transmitted through the Fabry-Pérot cavity. The laser frequency is scanned by simultaneously changing the diode laser current and the confocal cavity length, while the feedback loop keeps the optical path length between the laser and cavity optimized. The output of the laser transmitted through the beam splitter is used for beat note measurements against the FLFC, and for the atomic beam spectroscopy. Approximately 1 mW of the laser output is used for the beat note. A small portion of the laser output (several  $\mu\text{W}/\text{cm}^2$ ) is sent to the vacuum chamber

through a single-mode fiber and is used for atomic excitation. After the fiber, the probe beam is collimated to a diameter of 6.4 mm, and its polarization is aligned along the atomic beam axis with a polarizer (extinction ratio of 1/1000). In order to measure the deviation from  $\pi/2$  rad of the angle between the laser and the atomic beam, a corner cube is used to retroreflect the probe beam after it passes through the vacuum chamber. The uncertainty of the corner cube angle is specified to be less than  $9.7 \times 10^{-6}$  rad. The retroreflected beam overlaps the incident beam as it passes back through the chamber. At the tip of the corner cube the polarization is scrambled, so a polarizer with its axis aligned with the incident laser beam polarization is placed between the vacuum chamber and the corner cube. The intensity of the retroreflected beam inside the interaction region is 60% of that of the incident one due to losses from the chamber output window, the polarizer, and the corner cube. By comparing one-beam spectra with two-beam spectra, the direction of the laser beam with respect to that of the atomic beam can be steered using a piezoelectric-transducer (PZT) driven optical mount that is controlled by the computer.

### B. Atomic beam and fluorescence detection

The Cs beam is generated in a vacuum chamber containing a two stage oven. The oven consists of a reservoir and nozzle as described in Ref. [14]. The reservoir is heated to  $T=393$  K and the nozzle is kept at  $T=443$  K. The nozzle consists of a closely packed array of small stainless steel tubes that fill a rectangular hole in a stainless steel knife edge flange. As it emerges from the nozzle, the atomic beam has a rectangular profile, an angular divergence of a few degrees, and a density of  $2.6 \times 10^{13} \text{ cm}^{-3}$ . A stack of closely spaced microscope cover slips placed 12 cm down stream further collimates the atomic beam to an angular divergence of 12 mrad over the entire  $13 \text{ mm} \times 15 \text{ mm}$  profile. The final den-

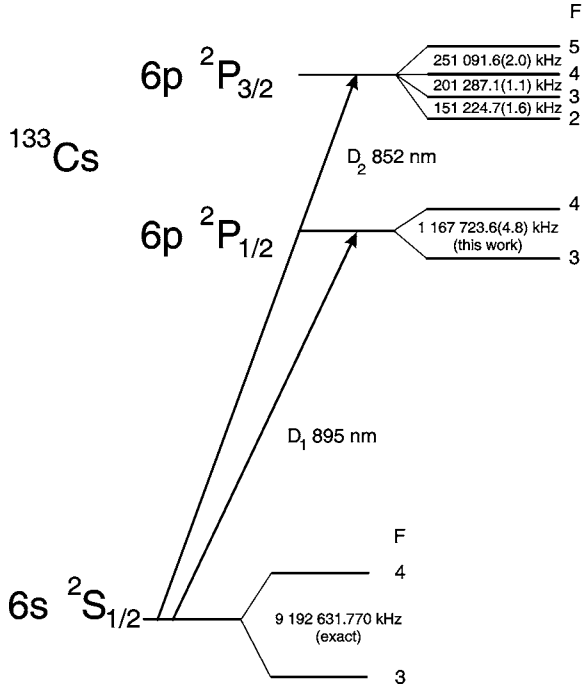


FIG. 2. Neutral  $^{133}\text{Cs}$  energy level diagram (not to scale).

sity at the laser interaction region is  $1.6 \times 10^{10} \text{ cm}^{-3}$ . At this density, collisional shifts and broadening are negligible [15]. The beam from the probe laser intersects the thermal beam at a right angle after the nozzle and above a large-area photodetector. The laser excites the  $6s \ ^2S_{1/2}(F_g=3,4) \rightarrow 6p \ ^2P_{1/2}(F_x=3,4)$  transitions in neutral  $^{133}\text{Cs}$ . The energy level diagram of the cesium atom is shown in Fig. 2. A curved gold mirror placed above the interaction region reflects the fluorescence of the excited atoms back onto the photodetector, increasing the collection efficiency. The photocurrent is turned into a voltage with a high-gain transimpedance amplifier, and the voltage is sampled by a computer with the DAQ board. In order to avoid shifts and distortion of the line shapes, the magnetic field in the interaction region is compensated to better than  $2 \times 10^{-6} \text{ T}$  by use of three pairs of helmholtz coils. To avoid the formation of a Cs cloud inside the vacuum chamber, a liquid nitrogen trap is used.

### C. Femtosecond laser frequency comb

To measure and scan the frequency of the probe laser, part of its output is mixed with the output of a self-referenced femtosecond laser frequency comb [16–18]. By use of established techniques [16,19,20], the frequency comb is referenced to a stable hydrogen maser that has its frequency calibrated by a cesium atomic fountain clock [21]. The fractional frequency instability of the comb teeth is equivalent to that of the hydrogen maser, given by  $\sim 2 \times 10^{-13} \tau^{-1/2}$ , with  $\tau$  the integration time measured in seconds. When averaged for several hours, the frequency of each tooth of the femtosecond comb can be known relative to the cesium primary frequency standard with uncertainties approaching a few parts in  $10^{15}$ . In this way, the optical frequency of the probe laser can be precisely determined by measuring the beat note be-

tween the probe laser and the component of the FLFC to which it is locked.

### III. THEORETICAL MODEL

The term “recoil shift” is used inconsistently in the literature and varies depending upon the particulars of the measurement being discussed. Therefore the description of the recoil energy shift that is relevant to the analysis of our results is given in detail here. The maximum probability for single photon absorption by an atom occurs when momentum and energy are conserved. Although the atoms in our apparatus are not moving particularly fast relative to the speed of light, the approach of using Lorentz invariant 4-vectors in this derivation is a natural way to maintain the relationship between the photon’s momentum and energy as well as its Doppler shift relative to the atom’s rest frame. In the laboratory frame with the atom initially in the ground state and moving with velocity  $\mathbf{v}_i$ , the initial state of the photon and atom can be described by the contravariant 4-vectors  $k^\alpha = (\omega/c, \mathbf{k})$  and  $p_i^\alpha = (\gamma_i m_g c, \mathbf{p}_i)$ , where  $\omega$  is the angular frequency of the photon in the laboratory,  $|\mathbf{k}| = \omega/c$ ,  $\gamma^{-1} = \sqrt{1 - \beta^2}$ ,  $\boldsymbol{\beta} = \mathbf{v}/c$ ,  $m_g$  is the rest mass the atom in the initial ground state, and  $\mathbf{p}_i = \gamma_i m_g \mathbf{v}_i$ . After the photon is absorbed, the 4-momentum of the atom in the excited state is  $p_f^\alpha = (\gamma_f m_x c, \mathbf{p}_f)$ , where  $m_x$  is the rest mass of the atom in the excited state and  $\mathbf{p}_f$  is its final momentum. Conservation of 4-momentum implies

$$p_i^\alpha + \hbar k^\alpha = p_f^\alpha. \quad (1)$$

Multiplying each side of Eq. (1) by its corresponding covariant 4-vector, one obtains the 4-vector magnitude

$$\begin{aligned} (p_i^\alpha + \hbar k^\alpha)(p_{i\alpha} + \hbar k_\alpha) &= p_i^\alpha p_{i\alpha} + \hbar p_i^\alpha k_\alpha + \hbar k^\alpha p_{i\alpha} + \hbar k^\alpha \hbar k_\alpha \\ &= p_f^\alpha p_{f\alpha}. \end{aligned} \quad (2)$$

Since the magnitude of the individual 4-vectors are Lorentz invariants  $p_f^\alpha p_{f\alpha} = m_x^2 c^2$ ,  $p_i^\alpha p_{i\alpha} = m_g^2 c^2$ ,  $k^\alpha k_\alpha = \omega^2/c^2 - \mathbf{k} \cdot \mathbf{k} = 0$ , Eq. (2) simplifies to

$$\begin{aligned} m_x^2 c^2 + 2\hbar(\omega \gamma_i m_g - \mathbf{k} \cdot \mathbf{p}_i) &= m_g^2 c^2 + 2\hbar(\omega \gamma_i m_g - \omega \gamma_i m_g \hat{\mathbf{k}} \cdot \boldsymbol{\beta}_i) \\ &= m_g^2 c^2, \end{aligned} \quad (3)$$

where we have used  $\mathbf{k} = (\omega/c)\hat{\mathbf{k}}$ . Rearranging, we obtain

$$\gamma_i \omega (1 - \hat{\mathbf{k}} \cdot \boldsymbol{\beta}_i) = \frac{m_x^2 c^4 - m_g^2 c^4}{2\hbar m_g c^2}, \quad (4)$$

where we assume  $m_x c^2 - m_g c^2$  to be the energy difference of the atomic levels in the rest frame of the atom and express this energy difference in terms of angular frequency  $\hbar(\omega_x - \omega_g) = E_x - E_g = m_x c^2 - m_g c^2$ . Substituting  $m_x c^2 = m_g c^2 + \hbar(\omega_x - \omega_g)$  into Eq. (4) gives the expression

$$\gamma_i \omega (1 - \hat{\mathbf{k}} \cdot \boldsymbol{\beta}_i) = \omega_x - \omega_g + \frac{\hbar(\omega_x - \omega_g)^2}{2m_g c^2}. \quad (5)$$

This expression is relativistically correct and has a simple interpretation. The term on the left-hand side is equal to the

laboratory frequency of the photon transformed into the rest frame of the atom, and the last term on the right-hand side is related to the kinetic energy of the recoiling atom after it has absorbed a single photon. Thus, properly accounting for the recoil energy shift, the maximum probability for single photon absorption occurs at the center of the Lorentzian line shape given by

$$L(\omega) = \frac{1}{\left[ \gamma_i \omega (1 - \hat{\mathbf{k}} \cdot \boldsymbol{\beta}_i) - \left( \omega_x - \omega_g + \frac{\hbar(\omega_x - \omega_g)^2}{2m_g c^2} \right) \right]^2 + \left( \frac{\Gamma}{2} \right)^2}, \quad (6)$$

where  $\Gamma = 1/\tau$  and  $\tau$  is the spontaneous emission lifetime of the excited state. In our experiment, we measure the photon frequency in the laboratory frame that produces the maximum fluorescence, which occurs when the probability for single photon absorption is maximized at the peak of the Lorentzian.

In recent works [22,23], it was discussed that the atomic recoil in a dispersive medium is  $n\hbar\mathbf{k}$ , where  $n$  is the index of refraction of the medium. In this case, the term in Eq. (6) related to the kinetic energy of the recoiling atom should depend on  $n^2$ , and so on the photon detuning from resonance as well as the atomic beam density. We calculated the effective line shape of the absorption resonance taking into account the excited state natural linewidth of 4.5629(26) MHz [5] and the index of refraction of the atomic beam at typical densities of  $1.6 \times 10^{10} \text{ cm}^{-3}$ . The resulting line shape is asymmetric because of the behavior of the index of refraction in the vicinity of the atomic resonance. When fitted with a symmetric function, the line center is offset from the Lorentzian line center calculated using Eq. (6). This offset is found to be negligible compared to our experimental resolution.

In our apparatus, the atoms effuse from the nozzle, kept at 443 K, with a most probable speed of about 300 m/s. Since  $\beta^2 \approx 10^{-12}$ , we can use  $\gamma \approx 1$ . The first order Doppler shift,  $\hat{\mathbf{k}} \cdot \boldsymbol{\beta}_i$ , is largely eliminated by collimating the atomic beam to a full angular divergence of  $\sim 12$  mrad and aligning the laser beam perpendicular to the atomic beam. The resulting velocity distribution convolved with the Lorentzian line shape yields a Voigt profile where the Lorentzian line width is comparable to the Gaussian width [14].

In the case of zero magnetic field, all Zeeman sublevels  $M_F$  of a specific ground- ( $F_g$ ) or excited- ( $F_x$ ) state component of the Cs atoms have the same energy, and a single Voigt profile can be used to describe all of them. If there is a static magnetic field present, each Voigt profile from a specific Zeeman sublevel pair ( $M_{F_g}, M_{F_x}$ ) will have a maximum at a different optical frequency. Also, optical pumping will generally occur, causing the initially uniform population of the Zeeman sublevels of the ground state to be redistributed, and the fluorescence amplitude of each Voigt profile will be different. In order to describe the fluorescence of a specific ground-state–excited-state pair ( $F_g, F_x$ ) with a single Voigt profile, the static magnetic field in the interaction region is

minimized to suppress Zeeman splitting, and the laser intensity kept low enough to reduce optical pumping. In our case, the background magnetic field in the interaction region is reduced to  $2 \times 10^{-6}$  T, and the laser intensity is kept on the order of  $2 \mu\text{W}/\text{cm}^2$ , or approximately 1/1000 of the saturation intensity of the  $6s \ ^2S_{1/2} \rightarrow 6p \ ^2P_{1/2}$  transition.

If the angle deviates from  $\pi/2$  rad, the Doppler effect causes shifts in the optical frequencies of all transitions. The approach used here is to keep the angle between the atomic beam and the laser beam as close to  $\pi/2$  rad as possible, as described in [24]. If there is a deviation from  $\pi/2$  rad, using a second counter-propagating beam creates two superimposed unresolved profiles with centers that differ by twice as much as the Doppler shift caused by the deviation. If these two-beam spectra are fitted with a single-profile function, the effective center is different from that obtained by fitting a one-beam spectrum. By minimizing this difference, the deviation of the angle between the laser and the atomic beam from  $\pi/2$  rad is also minimized, allowing the use of a single Voigt profile to obtain each of the line centers.

In the model, a dc offset accounts for the photodetector leakage current and laser scattered light. A linear slope parameter accounts for any slow change in the photodetector leakage current. The laser intensity is found to vary less than 0.5% over the entire scan interval. The measured spectrum consists of data points for which the optical frequency, the averaged fluorescence signal and the standard deviation of the fluorescence signal are recorded. The fitting program uses the standard deviation of each fluorescence measurement as a weighting factor. The Levenberg-Marquardt method of minimization is taken from [25].

## IV. MEASUREMENT PROTOCOL

### A. Frequency measurement

The  $6p \ ^2P_{1/2}$  excited state has two components, separated by 1.168 GHz due to the hyperfine interaction. The ground-state components are well separated by 9.193 GHz. The natural linewidth of the excited state is 4.5629(26) MHz [5]. The large separations allow the optical transition between each pair of ground ( $F_g$ ) and excited ( $F_x$ ) states to be measured separately. To determine the optical frequency of each pair, the probe laser is offset locked to a specific FLFC component, and is scanned within a 40 MHz broad interval by changing the offset frequency. The repetition rate and the offset frequency of the FLFC are chosen so that the optical frequency of the specific spectral component is in the center of the probe laser frequency scan. To perform the offset lock, the beat note between the probe laser and the comb component is mixed with the output of a rf synthesizer, referenced to the hydrogen maser. The offset lock maintains the difference between the synthesizer frequency,  $f_{\text{synth}}$ , and the probe laser-comb beat note,  $f_{\text{beat}}$ . When the computer scans the RF frequency synthesizer, the offset lock scans the probe laser to maintain the difference between  $f_{\text{synth}}$  and  $f_{\text{beat}}$ . The offset frequency is chosen to be approximately 30 MHz by adjusting the phase delay arm length of a frequency discriminator used in the offset lock scheme, as described in [26]. Instead of measuring the beat note between the probe laser and the

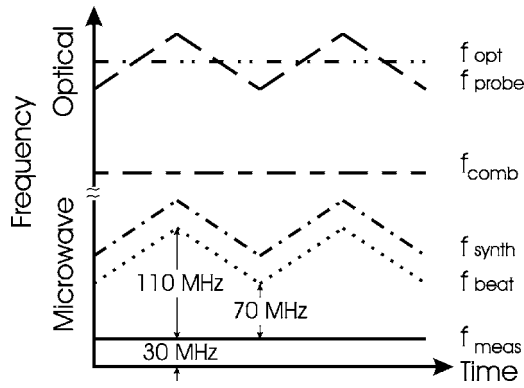


FIG. 3. Time diagram illustrating the temporal behavior of the probe laser frequency  $f_{\text{probe}}$  with respect to the comb component  $f_{\text{comb}}$  and the optical transition frequency  $f_{\text{opt}}$ . Also shown is the change of the different microwave frequencies: synthesizer frequency  $f_{\text{synth}}$ , beat note frequency  $f_{\text{beat}} = f_{\text{probe}} - f_N$ , and the measured frequency  $f_{\text{meas}}$ .

frequency comb, which changes as the probe laser is scanned, the difference  $f_{\text{meas}} = f_{\text{synth}} - f_{\text{beat}} \approx 30$  MHz, maintained by the offset lock, is measured. This signal has a signal-to-noise ratio of more than 30 dB in 300 kHz bandwidth. To avoid interference with the higher frequencies of the beat note and the synthesizer, bandpass and low-pass filters are used before the signal is sent to the frequency counter. The probe laser frequency can be either above or below the comb frequency component, so the measured frequency of the beat note is the absolute value of the frequency difference between the probe laser and the comb component  $f_{\text{beat}} = |f_{\text{comb}} - f_{\text{probe}}|$ . The sign is determined before the offset lock is turned on by observing the change in the beat note when the repetition rate is increased or decreased.

### B. Spectrum measurement

The measurements are done as follows. The probe laser frequency is roughly adjusted to the maximum of the optical transition  $6s^2S_{1/2}(F_g) \rightarrow 6p^2P_{1/2}(F_x)$  of interest. The optical frequency of the  $N$ th comb component is given by  $f_{\text{comb}} = \pm f_0 + Nf_{\text{rep}}$ , where  $f_0$  is the comb offset frequency and  $f_{\text{rep}}$  is the repetition rate on the order of 1 GHz. The rf synthesizer frequency is set to be 30 MHz above  $f_{\text{beat}}$  and the difference  $f_{\text{synth}} - f_{\text{beat}}$  is locked. The beat note  $f_{\text{beat}}$  is then scanned over the interval 70–110 MHz by changing the rf synthesizer frequency. The FLFC repetition rate  $f_{\text{rep}}$  is changed to make the laser frequency equal to the transition maximum when  $f_{\text{beat}} = |f_{\text{comb}} - f_{\text{probe}}| = 90$  MHz. A diagram of the temporal behavior of the different frequencies during a scan is shown in Fig. 3. Four scans of one-beam data are recorded, two with increasing, and two with decreasing laser frequency. Each scan consists of 100 data points with a frequency difference of 400 kHz between them. Subsequent to each frequency step, the fluorescence is measured in a 0.5 s interval with a rate of 2000 samples per second while the counter simultaneously measures  $f_{\text{meas}} = f_{\text{synth}} - f_{\text{beat}}$ . The counter performs statistics on four frequency measurements. The computer records  $f_{\text{synth}} - f_{\text{meas}} = f_{\text{beat}}$ , the averaged fluo-

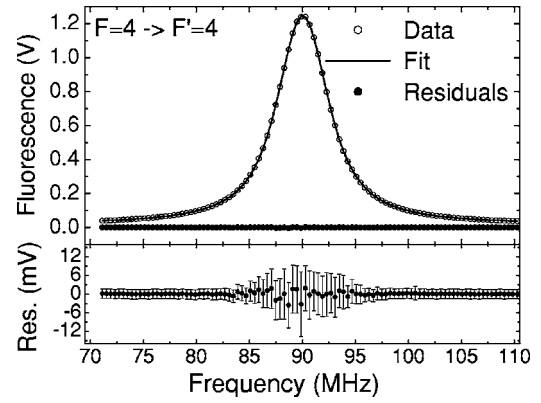


FIG. 4. Typical one-beam spectrum of  $6s^2S_{1/2}(F_g=4) \rightarrow 6p^2P_{1/2}(F_x=4)$  transition. Top plot: data—open circles; model—solid line; residuals—solid circles. Bottom plot: residuals—solid circles; with the standard deviation of each fluorescence data point given as error bar. The error in the mean for each point can be found by dividing the standard deviations by  $\sqrt{1000}$ .

rescence signal, and the standard deviation of the fluorescence signal. A typical one-beam spectrum of the  $6s^2S_{1/2}(F_g=4) \rightarrow 6p^2P_{1/2}(F_x=4)$  transition is shown in Fig. 4. The standard deviation of each fluorescence data point is shown as an error bar on the bottom graph of Fig. 4.

After the scan is performed, the retroreflected beam is sent into the interaction region and four two-beam scans are acquired as described. The two types of spectra (four scans each) are then fitted with the same one-beam model. A fit of the one-beam spectrum in Fig. 4 is also shown. The Doppler shift is canceled by minimizing the difference between the optical frequencies in one- and two-beam spectra. All line centers for one-beam data for which the difference in the centers between the one and two laser beam configurations is less than 3 kHz are used to determine the Doppler shift-free optical frequency.

## V. RESULTS AND DATA ANALYSIS

### A. Optical frequency determination

Toward determining the unperturbed or shift-free optical frequencies, the spectral line centers are extrapolated to zero laser intensity by collecting data at different intensities for both beam configurations. The experimentally determined intensity-dependent shifts are listed in rows 1 and 2 of Table I. These corrections compensate for shifts due to optical pumping, Zeeman effect, and multiple-photon recoils. The few atoms that might absorb an additional photon shift the peak center by a negligible amount for which the intensity adjustment compensates [27]. Since the  $6s^2S_{1/2} \rightarrow 6p^2P_{1/2}$  transitions are open and the atoms can decay to the ground state component which is not accessible to the laser, all intensity-dependent shifts are smaller than, for example, the ones observed for the closed transitions for the  $6s^2S_{1/2} \rightarrow 6p^2P_{3/2}$  transition [24].

Also listed in Table I are the uncertainties in the optical frequencies due to other systematic effects. Frequency shifts due to the Zeeman effect are measured by applying one at a

TABLE I. Systematic corrections and uncertainties in kilohertz units. [(1) One-beam data; (2) Two-beam data]. For the intensity dependent shift (rows 1 and 2), the correction that has to be made to the optical frequency values when extrapolating to zero laser intensity is shown. The uncertainty associated with this correction is given in parentheses.

	3→3	3→4	4→3	4→4
(1) Intensity dependent shift	0.6(0.5)	1.3(0.6)	0.7(0.7)	0.1(0.7)
(2) Intensity dependent shift	0.1(0.6)	0.5(0.7)	0.9(1.0)	0.5(1.1)
Zeeman effect	±0.5	±0.5	±0.5	±0.5
AC Stark shift	<0.1	<0.1	<0.1	<0.1

time a dc magnetic field of  $1 \times 10^{-4}$  T in each of the three spatial directions. From the shifts measured, an upper limit of 0.5 kHz is placed on the Zeeman frequency shift caused by the maximum residual dc magnetic field of  $2 \times 10^{-6}$  T in the interaction region, as listed in row 3 of Table I. At an intensity of  $2 \mu\text{W}/\text{cm}^2$ , the ac Stark shift is calculated to be less than 100 Hz, as listed in row 4 of Table I. The density-dependent shift is estimated to be negligible at the given atomic beam density. Also, the atomic density was changed by a factor of two without measurable effect on the optical frequencies.

In our previous optical frequency measurement [24], the uncertainty in the optical frequencies given by the corner cube angle imperfection was assumed to be the one specified by the manufacturer,  $9.7 \times 10^{-6}$  rad. In the present experiment, it was found that rotating the corner cube by  $\pi$  rad produces a shift of 1.1(1.0) kHz; however, this systematic effect was eliminated from our present data. For half of all measurements, the corner cube was rotated by  $\pi$  rad before minimizing the laser-atomic beam misalignment.

The data for each of the four optical transitions ( $F_g=3, 4 \rightarrow F_x=3, 4$ ) were collected over a period of several months. The fitted line centers were extrapolated to zero laser intensity using the measured shifts given in rows 1 and 2 of Table I. The zero-intensity optical frequencies for the one- ( $f_{1b}$ ) and two-beam ( $f_{2b}$ ) configurations were used to determine the Doppler-free values using the relation

$$f_{\text{zero}} = f_{1b} - (f_{1b} - f_{2b})a, \quad (7)$$

where  $a=1.3(2)$  is an experimentally measured parameter [27], which depends on the ratio between the two laser beam intensities.

The uncertainty for each scan is the quadrature combination [according to Eq. (7)] of the one- and two-beam fit uncertainties, the uncertainties of the intensity extrapolation (rows 1 and 2 of Table I), and the Zeeman effect uncertainty (row 3 of Table I). The weighted mean value and the weighted average variance for each optical frequency are given in rows 1 and 2 of Table II.

### B. Systematic checks

One possible check of the validity of our optical frequency values is to compare the frequency separation be-

TABLE II. Optical frequencies between different components of the  $6s^2S_{1/2}(F_g=3,4) \rightarrow 6p^2P_{1/2}(F_x=3,4)$  transition, measured in kilohertz units. Rows 1 and 2 represent weighted averages of the measured values. Rows 3 and 4 represent the values obtained by least-squares minimization of the values in Rows 1 and 2 using the ground-state HFS splitting  $\Delta\nu_{6s_{1/2}}$  as a constraint, and the line centroid  $f_{D1}$  and the excited state HFS splitting  $\Delta\nu_{6p_{1/2}}$  as unknowns.

	$F_x=3$	$F_x=4$
Meas. $F_g=3$	335 120 562 759.7(4.9)	335 121 730 483.2(5.3)
Meas. $F_g=4$	335 111 370 130.2(4.6)	335 112 537 853.9(4.0)
Least-sq. $F_g=3$	335 120 562 760.8(3.4)	335 121 730 484.4(3.3)
Least-sq. $F_g=4$	335 111 370 129.1(3.4)	335 112 537 852.7(3.3)

tween the excited- and ground-state components due to the hyperfine structure (HFS). Two such checks are possible using different optical transitions. One is to compare the excited-state frequency splitting by subtracting the optical frequencies of the transitions for which the laser excites the same ground-state component  $F_g$  but different excited-state components. Another check is to compare the optical frequencies of the transitions for which the laser excites the same excited-state component  $F_x$  but different ground-state components, and compare the difference with the ground-state splitting that is used as the definition of the second [28]. From the optical frequency measurements, the following results are obtained:

$$f_{34} - f_{33} = \Delta\nu_{6p_{1/2}} = 1\,167\,723.5(7.3) \text{ kHz}$$

$$f_{44} - f_{43} = \Delta\nu_{6p_{1/2}} = 1\,167\,723.7(6.1) \text{ kHz}$$

$$f_{33} - f_{43} - \Delta\nu_{6s_{1/2}} = -2.3(6.8) \text{ kHz}$$

$$f_{34} - f_{44} - \Delta\nu_{6s_{1/2}} = -2.5(6.7) \text{ kHz}, \quad (8)$$

where  $f_{gx}$  is the optical frequency of the transition between  $F_g \equiv g$  ground and  $F_x \equiv x$  excited-state component,  $\Delta\nu_{6p_{1/2}}$  is the hyperfine splitting of the  $6p^2P_{1/2}$  excited state, and  $\Delta\nu_{6s_{1/2}}$  is the hyperfine splitting of the  $6s^2S_{1/2}$  ground state. The excellent internal consistency suggests that there is no significant underestimation of the uncertainties.

### C. $D_1$ line centroid and $6p^2P_{1/2}$ state HFS splitting

Our direct measurements consist of the four optical frequencies given in the top two rows of Table II. Each value corresponds to the frequency of the photon required to make a transition from a particular ground-state hyperfine level to a particular excited-state hyperfine level with maximum probability, and we label these frequencies as  $f_{gx}$ . These frequencies differ from the frequency corresponding to the energy difference between a pair of atomic levels,  $(E_x - E_g)/h = f_x - f_g$ , as derived in Eq. (5)

$$f_{gx} = f_x - f_g + \frac{h(f_x - f_g)^2}{2m_g c^2}. \quad (9)$$

The difference in the energy between the excited state atom at rest and the ground-state atom at rest can be expressed as the difference between their respective energy centroids expressed as a frequency  $f_c$  plus the difference in their respective shifts due to the presence of the hyperfine interaction,  $f_{\text{HF}x} - f_{\text{HF}g}$

$$f_x - f_g = f_c + f_{\text{HF}x} - f_{\text{HF}g}. \quad (10)$$

We note that in substituting Eq. (10) into Eq. (9), the photon frequency has a different recoil energy shift for each pair of excited- and ground-state hyperfine levels

$$f_{gx} = f_c + f_{\text{HF}x} - f_{\text{HF}g} + \frac{hf_c^2}{2m_g c^2} \left[ 1 + 2 \frac{(f_{\text{HF}x} - f_{\text{HF}g})}{f_c} + \frac{(f_{\text{HF}x} - f_{\text{HF}g})^2}{f_c^2} \right]. \quad (11)$$

However, the contribution to the recoil due to the hyperfine shifts is less than 1 Hz in all cases, so we consider only the recoil contribution due to the line centroid

$$f_{gx} \approx f_c + f_{\text{HF}x} - f_{\text{HF}g} + \frac{hf_c^2}{2m_g c^2}. \quad (12)$$

With this simplification, the four optical frequencies involved are theoretically related to two unknown parameters: the energy centroid,  $f_c$  and the excited-state hyperfine splitting  $\Delta f_{\text{HF}x}$  and one known constraint, the  $^{133}\text{Cs}$  ground-state hyperfine splitting  $\Delta f_{\text{HF}g}$

$$\begin{aligned} f_{44} &= \left( f_c + \frac{hf_c^2}{2m_g c^2} \right) + \frac{7}{16} \Delta f_{\text{HF}x} - \frac{7}{16} \Delta f_{\text{HF}g} \\ f_{34} &= \left( f_c + \frac{hf_c^2}{2m_g c^2} \right) + \frac{7}{16} \Delta f_{\text{HF}x} + \frac{9}{16} \Delta f_{\text{HF}g} \\ f_{43} &= \left( f_c + \frac{hf_c^2}{2m_g c^2} \right) - \frac{9}{16} \Delta f_{\text{HF}x} - \frac{7}{16} \Delta f_{\text{HF}g} \\ f_{33} &= \left( f_c + \frac{hf_c^2}{2m_g c^2} \right) - \frac{9}{16} \Delta f_{\text{HF}x} + \frac{9}{16} \Delta f_{\text{HF}g}. \end{aligned} \quad (13)$$

Our directly measured optical frequencies from Table II are

$$\begin{aligned} f_{44}^m &= 335\,112\,537\,853.9(4.0) \text{ kHz} \\ f_{34}^m &= 335\,121\,730\,483.2(5.3) \text{ kHz} \\ f_{43}^m &= 335\,111\,370\,130.2(4.6) \text{ kHz} \\ f_{33}^m &= 335\,120\,562\,759.7(4.9) \text{ kHz}. \end{aligned} \quad (14)$$

The system of four equations and two unknowns is overdetermined. Therefore, we perform a least-squares reduction analysis to find the most probable values for  $f_c + hf_c^2/2m_g c^2$  and  $\Delta f_{\text{HF}x}$  by minimizing the sum of the deviations

$$\chi^2 = (f_{44}^m - f_{44})^2 + (f_{34}^m - f_{34})^2 + (f_{43}^m - f_{43})^2 + (f_{33}^m - f_{33})^2 \quad (15)$$

with respect to these two unknowns to obtain the following expressions:

$$\begin{aligned} \Delta f_{\text{HF}x} &= \frac{f_{44}^m + f_{34}^m}{2} - \frac{f_{43}^m + f_{33}^m}{2} = 1\,167\,723.6(4.8) \text{ kHz} \\ \left( f_c + \frac{hf_c^2}{2m_g c^2} \right) &= \frac{9}{16} \frac{f_{44}^m + f_{34}^m}{2} + \frac{7}{16} \frac{f_{43}^m + f_{33}^m}{2} - \frac{1}{16} \Delta f_{\text{HF}g} \\ &= 335\,116\,048\,750.0(2.4) \text{ kHz}. \end{aligned} \quad (16)$$

Substituting into Eq. (16) the four measured optical frequencies and using standard error propagation techniques, we obtain the values given at the right. Solving for  $f_c$ , we obtain the frequency centroid of the transition

$$f_c = 335\,116\,048\,748.1(2.4) \text{ kHz}. \quad (17)$$

Note that the definition of the frequency centroid used here excludes the shift of  $hf_c^2/2m_g c^2 = 1.9$  kHz, which is due to the momentum imparted to a cesium atom by absorption of a single photon.

The values for  $f_c + hf_c^2/2m_g c^2$  and  $\Delta f_{\text{HF}x}$  can also be substituted into Eq. (13) to obtain our final least-squares consistent experimental values

$$\begin{aligned} f_{44} &= \left( f_c + \frac{hf_c^2}{2m_g c^2} \right) + \frac{7}{16} \Delta f_{\text{HF}x} - \frac{7}{16} \Delta f_{\text{HF}g} \\ &= 335\,112\,537\,852.7(3.3) \text{ kHz} \\ f_{34} &= \left( f_c + \frac{hf_c^2}{2m_g c^2} \right) + \frac{7}{16} \Delta f_{\text{HF}x} + \frac{9}{16} \Delta f_{\text{HF}g} \\ &= 335\,121\,730\,484.4(3.3) \text{ kHz} \\ f_{43} &= \left( f_c + \frac{hf_c^2}{2m_g c^2} \right) - \frac{9}{16} \Delta f_{\text{HF}x} - \frac{7}{16} \Delta f_{\text{HF}g} \\ &= 335\,111\,370\,129.1(3.4) \text{ kHz} \\ f_{33} &= \left( f_c + \frac{hf_c^2}{2m_g c^2} \right) - \frac{9}{16} \Delta f_{\text{HF}x} + \frac{9}{16} \Delta f_{\text{HF}g} \\ &= 335\,120\,562\,760.8(3.4) \text{ kHz}. \end{aligned} \quad (18)$$

The directly measured optical frequencies and the least-squares-reduced values appear for comparison in Table II. The least-squares value of the excited-state hyperfine splitting  $\Delta f_{\text{HF}x}$  is given in Table III together with previous measurements.

## VI. DETERMINATION OF THE FINE-STRUCTURE CONSTANT

### A. Recomputing $h/mc_s$

The fine-structure constant  $\alpha$  permeates physics, and its precision has driven both theory and experiment now for

TABLE III. Hyperfine structure splitting of  $6p^2P_{1/2}$  excited state, measured in kilohertz.

1 167 723.6(4.8)	This work
1 167 688(81)	Udem <i>et al.</i> [3]
1 167 540(320)	Rafac and Tanner [29]

almost 100 years [27]. Since 1985, the value of  $\alpha$  has been dominated by the value obtained from the anomalous magnetic moment of the electron, which now has an uncertainty of  $3.8 \times 10^{-9}$ . However, the measurements of the magnetic moment of the electron must be combined with substantial but improving QED calculations. The cesium system provides a way of obtaining a competitive value of alpha that is QED free. The preliminary results for  $h/m_{\text{Cs}}$  reported in 2002 by Wicht *et al.* [1] using an atom interferometer gave a value of  $\alpha$  precise enough to be used in the (CODATA) determination of recommended values of the fundamental constants [30]. This value of  $\alpha$  had an uncertainty of  $7.7 \times 10^{-9}$ . Since the determination of  $\alpha$  from cesium depends upon the  $^{133}\text{Cs}$  D<sub>1</sub> transition frequencies, and our measurements disagree with the best previously reported measurements (by 1.4 combined standard deviations), we are compelled to report a revised value for  $\alpha$ .

Wicht *et al.* [1] used an atom interferometer to measure the frequency shift of an atomic resonance due to recoil after the atom interacts with an integer number of photons. In their experiment, cesium atoms are first prepared in a single ground state hyperfine level that can be described by  $p_i^\alpha = (\gamma_i m_g c, \mathbf{p}_i)$ . The atoms then interact with one pair of photons, which transfers the atomic population from one hyperfine ground state to another by absorption,  $k_A^\alpha = (\omega_A/c, \mathbf{k}_A)$ , then stimulated emission,  $k_B^\alpha = (\omega_B/c, \mathbf{k}_B)$ . Next the atoms interact with a second pair of photons that transfers the atomic population back to the initial ground state hyperfine level through absorption,  $k_B'^\alpha = (\omega_B'/c, \mathbf{k}_B')$ , then stimulated emission,  $k_A'^\alpha = (\omega_A'/c, \mathbf{k}_A')$ . In the end, the atoms have interacted with four photons and are back in their initial atomic state but have a different momentum,  $p_f^\alpha = (\gamma_f m_g c, \mathbf{p}_f)$ . The resonance condition for this four-photon process is given by energy and momentum conservation, which is easily represented in terms of 4-vectors

$$p_i^\alpha + \hbar k_A^\alpha + \hbar k_B'^\alpha = p_f^\alpha + \hbar k_A'^\alpha + \hbar k_B^\alpha, \quad (19)$$

where the left-hand side represents incoming particles and the right-hand side represents out-going particles. Solving for  $p_f^\alpha$ , taking the 4-vector magnitude on both sides, and rearranging gives

$$\begin{aligned} & 2\hbar[(k_A - k_B) - (k_A' - k_B')]^\alpha p_{i\alpha} \\ & + \hbar^2[(k_A - k_B) - (k_A' - k_B')]^\alpha [(k_A - k_B) - (k_A' - k_B')]_\alpha \\ & = p_f^\alpha p_{f\alpha} - p_i^\alpha p_{i\alpha} = 0, \end{aligned} \quad (20)$$

where all of the  $p_i$ ,  $p_f$ ,  $k_A$  and  $k_B$  are 4-vectors. Using  $p_f^\alpha p_{f\alpha} = m_g^2 c^2 = p_i^\alpha p_{i\alpha}$  leaves zero on the right-hand side. Rearranging and writing the result in terms of known parameters and those measured in the laboratory frame, we find

$$\begin{aligned} & 2\gamma_i m_g \{[(\omega_A - \omega_B) - (\omega_A' - \omega_B')] - [(\mathbf{k}_A - \mathbf{k}_B) - (\mathbf{k}_A' - \mathbf{k}_B')] \cdot \mathbf{v}_i\} \\ & = -\hbar[(k_A - k_B) - (k_A' - k_B')]^\alpha [(k_A - k_B) - (k_A' - k_B')]_\alpha. \end{aligned} \quad (21)$$

Solving for the frequency difference between the photon pairs and expanding the 4-vector product of the photon  $k$  vectors gives

$$\begin{aligned} (\omega_A - \omega_B) - (\omega_A' - \omega_B') & = [(\mathbf{k}_A - \mathbf{k}_B) - (\mathbf{k}_A' - \mathbf{k}_B')] \cdot \mathbf{v}_i \\ & + \frac{\hbar}{\gamma_i m_g c^2} [\omega_A \omega_B (1 - \hat{\mathbf{k}}_A \cdot \hat{\mathbf{k}}_B) \\ & + \omega_A \omega_A' (1 - \hat{\mathbf{k}}_A \cdot \hat{\mathbf{k}}_A') \\ & - \omega_A \omega_B' (1 - \hat{\mathbf{k}}_A \cdot \hat{\mathbf{k}}_B') \\ & - \omega_B \omega_A' (1 - \hat{\mathbf{k}}_B \cdot \hat{\mathbf{k}}_A') \\ & + \omega_B \omega_B' (1 - \hat{\mathbf{k}}_B \cdot \hat{\mathbf{k}}_B') \\ & + \omega_A' \omega_B' (1 - \hat{\mathbf{k}}_A' \cdot \hat{\mathbf{k}}_B')]. \end{aligned} \quad (22)$$

In the recoil measurement experiment, the unit vectors are chosen such that  $\hat{\mathbf{k}}_B = -\hat{\mathbf{k}}_A$ ,  $\hat{\mathbf{k}}_B' = \hat{\mathbf{k}}_A'$ , and  $\hat{\mathbf{k}}_A' = -\hat{\mathbf{k}}_A$ . Thus the resonance condition for the two two-photon processes is

TABLE IV. Physical constants used to calculate the value of alpha.

Constant	Value	Precision	Reference
Speed of light $c$	299 792 458 m/s	Exact	
Rydberg constant $R_\infty$	10 973 731.568 525(73) m <sup>-1</sup>	$6.6 \times 10^{-12}$	[30]
Recoil shift $f_{\text{rec}}/2$	15 006.276 88(23) Hz	$15\,000 \times 10^{-12}$	[1]
Electron mass $m_e$	$5.485\,799\,0945(24) \times 10^{-4}$ u	$440 \times 10^{-12}$	[30,32]
Cesium atomic mass $m_{\text{Cs}}$	132.905 451 931(27) u	$200 \times 10^{-12}$	[30,33]
Opt. frequency $f_{33} + f_{43}$	670 231 932 889.9(4.8) kHz	$7 \times 10^{-12}$	This work
Unified atomic mass unit $u$	$1.660\,538\,86(28) \times 10^{-27}$ kg	$1.7 \times 10^{-7}$	[30]
Value of $\alpha^{-1}$	137.036 000 0(11)	$7.7 \times 10^{-9}$	This work

$$(\omega_A - \omega_B) - (\omega'_A - \omega'_B) = (\omega_A + \omega_B + \omega'_A + \omega'_B) \hat{\mathbf{k}}_A \cdot \boldsymbol{\beta}_i + \frac{2\hbar}{\gamma_i m_g c^2} (\omega_A \omega_B + \omega_A \omega'_A + \omega_B \omega'_B + \omega'_A \omega'_B). \quad (23)$$

This expression is relativistically correct; however, several simplifications can be made. The left-hand side contains the frequency difference between the first two-photon resonance and the second two-photon resonance measured by Young [31] and Wicht *et al.* [1]. Since their atom interferometer uses laser cooled atoms in an atomic fountain, the initial atomic velocities are small, and one can make the approximation  $\gamma_i \approx 1$ . However, an initial atomic velocity does result in the first-order Doppler shift term on the right-hand side, which they eliminated experimentally by reversing all of the photon directions, i.e.,  $\hat{\mathbf{k}}_A \rightarrow -\hat{\mathbf{k}}_A$ , and averaging the results

$$(\omega_A - \omega_B) - (\omega'_A - \omega'_B) = \frac{2\hbar}{m_g c^2} (\omega_A \omega_B + \omega_A \omega'_A + \omega_B \omega'_B + \omega'_A \omega'_B). \quad (24)$$

If we make the substitutions  $\omega'_A = \omega_A - \Delta\omega_A$  and  $\omega'_B = \omega_B - \Delta\omega_B$ , then we obtain the following equation, where we easily see the simplification that occurs by keeping only the lowest order term on the right-hand side:

$$\begin{aligned} (\omega_A - \omega_B) - (\omega'_A - \omega'_B) &= \frac{2\hbar(\omega_A + \omega_B)^2}{m_g c^2} \\ &\times \left[ 1 - \frac{\Delta\omega_A + \Delta\omega_B}{\omega_A + \omega_B} + \frac{\Delta\omega_A \Delta\omega_B}{(\omega_A + \omega_B)^2} \right] \\ &\approx \frac{2\hbar(\omega_A + \omega_B)^2}{m_g c^2}. \end{aligned} \quad (25)$$

This result agrees with Young's Eqs. (2.30) and (2.31) in Ref. [31] and is used by Mohr and Taylor in Ref. [30]. This derivation, however, reveals where approximations are being made. When the result of Eq. (25) is expressed in units of frequency, the left-hand side is the recoil frequency defined by Mohr and Taylor in Ref. [30], and the right-hand side contains the optical photon frequencies given by our results in Eq. (18)

$$f_{\text{rec}} = \frac{2h}{m_{\text{Cs}} c^2} (f_{33} + f_{43})^2. \quad (26)$$

Wicht *et al.* reported the cesium atomic recoil as  $f_{\text{rec}}/2 = 15\,006.276\,88(23)$  Hz, where we are using the definition of  $f_{\text{rec}}$  used by Mohr and Taylor [30]. However, Mohr and Taylor [30] used the value  $f_{33} + f_{43} = 670\,231\,933\,044(81)$  kHz reported by Udem *et al.* [3]. We now use our value,  $f_{33} + f_{43} = 670\,231\,932\,889.9(4.8)$  kHz to obtain a new value for  $h/m_{\text{Cs}} = 3.002\,369\,432(46) \times 10^{-9}$  m<sup>2</sup>/s, which can be compared to the value given by Mohr and Taylor,  $h/m_{\text{Cs}} = 3.002\,369\,430(46) \times 10^{-9}$  m<sup>2</sup>/s. Mohr and Taylor assumed that the frequency uncertainties in [3] were highly correlated due to Zeeman effects and added the uncertainties linearly, whereas we added ours quadratically. The uncertainty of  $h/m_{\text{Cs}}$  remains about  $15 \times 10^{-9}$  due to the uncertainty in  $f_{\text{rec}}$ .

## B. Recomputing alpha from the cesium system

Alpha can be related to other fundamental constants through the equation

$$\alpha^2 = \frac{2R_\infty h}{c m_e} = \frac{2R_\infty m_p m_{\text{Cs}}}{c m_e m_p m_{\text{Cs}}} \frac{h}{m_{\text{Cs}}}. \quad (27)$$

However,  $m_p$ ,  $m_e$ , and  $m_{\text{Cs}}$  in kilograms have uncertainties of  $170 \times 10^{-9}$  or more, so mass ratios or masses in atomic units are utilized. The equation used in the CODATA 2002 determination was:  $h/m(^{133}\text{Cs}) \doteq A_r(e) c \alpha^2 / A_r(^{133}\text{Cs}) 2R_\infty$ , where the left-hand side is an experimental measurement used to adjust the constants on the right-hand side. The speed of light  $c$  is defined exactly,  $R_\infty$  was set to a fixed value ( $R_\infty = 10\,973\,731.568\,525(73)$  m<sup>-1</sup>) early in the CODATA adjustment procedure, and the uncertainties in the atomic mass of both the electron and the cesium atom are such that their uncertainties dominate. In a technical sense the atomic mass of the proton does not appear, but in a practical sense it is used in the experiments that determine the relative masses of the electron and the cesium atom. Improvements in precision for the masses for both the electron  $A_r(e) = 5.485\,799\,0945(24) \times 10^{-4}$  u and the cesium atom  $A_r(^{133}\text{Cs}) = 132.905\,451\,931(27)$  u were used in the CODATA 2002 determination [30] based on recent work [32,33]. Such changes can make it difficult to compare different determinations of alpha. The mass of the proton remained  $A_r(p) = 1.007\,276\,466\,88(13)$  u ( $130 \times 10^{-12}$ ) in the CODATA 2002 determination. Using 2002 CODATA values we obtain the result  $\alpha^{-1} = 137.036\,0000(11)$  with an uncertainty of  $7.7 \times 10^{-9}$  from the cesium atomic recoil measurements.

## VII. CONCLUSIONS

We have significantly improved the determination of the four absolute optical frequencies required to drive all possible single-photon hyperfine components of the  $6s\,^2S_{1/2} \rightarrow 6p\,^2P_{1/2}$  transition in atomic  $^{133}\text{Cs}$ . We have reached a precision of less than 4 kHz by improving upon both the precision and accuracy of previous work. The known values for the resonances make excellent and easily realizable laboratory optical frequency standards. Our results have allowed us to calculate other values for the cesium  $D_1$  centroid and the hyperfine splitting of the  $6p\,^2P_{1/2}$  state. Finally, our results play a significant role in determining the value of the fine-structure constant by the use of the cesium recoil measurement technique.

## ACKNOWLEDGMENTS

The authors thank Jim Bergquist and Rich Fox for helpful discussions, and Jim Bergquist and Jun Ye for carefully reading the manuscript. This project is supported by the Division of Chemical Sciences, Office of Basic Energy Sciences, Office of Energy Research, US Department of Energy under contract number DE-FG02-95ER14579 and by the National Science Foundation under Grant No. PHY99-87984.

- [1] A. Wicht *et al.*, Phys. Scr., T **102**, 82 (2002).
- [2] C. S. Wood *et al.*, Science **275**, 1759 (1997).
- [3] T. Udem *et al.*, Phys. Rev. Lett. **82**, 3568 (1999).
- [4] V. Gerginov, A. Derevianko, and C. E. Tanner, Phys. Rev. Lett. **91**, 072501 (2003).
- [5] C. Amiot, *et al.*, Phys. Rev. A **66**, 052506 (2002).
- [6] M. S. Safronova, W. R. Johnson, and A. Derevianko, Phys. Rev. A **60**, 4476 (1999).
- [7] A. Peters, K. Y. Chung, and S. Chu, Metrologia **38**, 25 (2001).
- [8] J. Ye *et al.*, Opt. Lett. **21**, 1280 (1996).
- [9] J. Helmcke *et al.*, IEEE Trans. Instrum. Meas. **52**, 250 (2003).
- [10] P. C. Pastor, Phys. Rev. Lett. **92**, 023001 (2004).
- [11] G. Ferrari *et al.*, Phys. Rev. Lett. **91**, 243002 (2003).
- [12] A. Marian *et al.*, Science **306**, 2063 (2004).
- [13] B. Dahmani, L. Hollberg, and R. Drullinger, Opt. Lett. **12**, 876 (1987).
- [14] V. Gerginov and C. E. Tanner, Opt. Commun. **222**, 17 (2003).
- [15] V. Vuletić *et al.*, Opt. Commun. **99**, 185 (1993).
- [16] T. M. Ramond *et al.*, Opt. Lett. **27**, 1842 (2002).
- [17] S. A. Diddams *et al.*, IEEE J. Sel. Top. Quantum Electron. **9**, 1072 (2003).
- [18] A. Bartels and H. Kurz, Opt. Lett. **27**, 1839 (2002).
- [19] T. Udem *et al.*, Phys. Rev. Lett. **86**, 4996 (2001).
- [20] D. J. Jones *et al.*, Science **288**, 635 (2000).
- [21] S. R. Jefferts *et al.*, Metrologia **39**, 321 (2002).
- [22] M. P. Haugan and F. V. Kowalski, Phys. Rev. A **25**, 2102 (1982).
- [23] G. K. Campbell *et al.*, Phys. Rev. Lett. **94**, 170403 (2005).
- [24] V. Gerginov *et al.*, Phys. Rev. A **70** 042505 (2004).
- [25] W. H. Press *et al.*, *Numerical Recipes in FORTRAN*, 2nd ed. (Cambridge University Press, New York, 1992).
- [26] V. Gerginov and C. E. Tanner, Opt. Commun. **216**, 391 (2003).
- [27] K. G. Calkins, Ph.D. thesis, University of Notre Dame, 2005.
- [28] Defined by international agreement (1967).
- [29] R. J. Rafac and C. E. Tanner, Phys. Rev. A **56**, 1027 (1997).
- [30] P. J. Mohr and B. N. Taylor, Rev. Mod. Phys. **77**, 1 (2005).
- [31] B. C. Young, Ph.D. thesis, Stanford University, 1997.
- [32] T. Beier *et al.*, Phys. Rev. Lett. **88**, 011603 (2002).
- [33] M. P. Bradley *et al.*, Phys. Rev. Lett. **83**, 4510 (1999).